Published in final edited form as:
Neuron. 2013 November 20; 80(4): . doi:10.1016/j.neuron.2013.08.023.

A unique population of ventral tegmental area neurons inhibits the lateral habenula to promote reward

Alice M. Stamatakis[1,2,3], **Joshua H. Jennings**[1,2,3], **Randall L. Ung**[2], **Grace A. Blair**[2], **Richard J. Weinberg**[3,4], **Rachael L. Neve**[5], **Frederick Boyce**[6], **Joanna Mattis**[7], **Charu Ramakrishnan**[7], **Karl Deisseroth**[7], and **Garret D. Stuber**[1,2,3,4,8,#]

[1]Neurobiology Curriculum, University of North Carolina at Chapel Hill, Chapel Hill, NC 27514, USA

[2]Department of Psychiatry, University of North Carolina at Chapel Hill, Chapel Hill, NC 27514, USA

[3]Neuroscience Center, University of North Carolina at Chapel Hill, Chapel Hill, NC 27514, USA

[4]Department of Cell Biology and Physiology, University of North Carolina at Chapel Hill, Chapel Hill, NC 27514, USA

[5]Department of Brain and Cognitive Science, Massachusetts Institute of Technology, Cambridge, MA 02139, USA

[6]Department of Neurology, Massachusetts General Hospital, Boston, MA 02114, USA

[7]Department of Bioengineering, Stanford University, Stanford, CA 94305, USA

[8]Bowles Center for Alcohol Studies, University of North Carolina at Chapel Hill, Chapel Hill, NC 27514, USA

Summary

Lateral habenula (LHb) neurons convey aversive and negative reward conditions through potent indirect inhibition of ventral tegmental area (VTA) dopaminergic neurons. While VTA dopaminergic neurons reciprocally project to the LHb, the electrophysiological properties and the behavioral consequences associated with selective manipulations of this circuit are unknown. Here, we identify a novel inhibitory input to the LHb arising from a unique population of VTA neurons expressing dopaminergic markers. Optogenetic activation of this circuit resulted in no detectable dopamine release in LHb brain slices. Instead, stimulation produced GABA-mediated inhibitory synaptic transmission, which suppressed the firing of postsynaptic LHb neurons in brain slices and increased the spontaneous firing rate of VTA dopaminergic neurons *in vivo*. Furthermore, *in vivo* activation of this pathway produced reward-related phenotypes that were dependent on intra-LHb $GABA_A$ receptor signaling. These results suggest that non-canonical inhibitory signaling by these hybrid dopaminergic-GABAergic neurons act to suppress LHb output under rewarding conditions.

[#]Address correspondence to: Garret D. Stuber, Ph.D., Assistant Professor, Departments of Psychiatry & Cell Biology and Physiology, UNC Neuroscience Center, University of North Carolina at Chapel Hill, Tel: +1 (919) 843-7140, Fax: +1 (919) 966-1050, gstuber@med.unc.edu.

Introduction

Dopaminergic neurons in the ventral tegmental area (VTA) are thought to encode reward prediction error - the difference between an expected reward and actual reward. Consistent with this, dopaminergic neurons are phasically excited by rewards and the cues that predict them, and are phasically inhibited by the omission of rewards and aversive stimuli (Cohen et al., 2012; Matsumoto and Hikosaka, 2007; Pan et al., 2005; Schultz et al., 1997; Tobler et al., 2005; Ungless et al., 2004). Increased firing rate of dopaminergic neurons in response to salient stimuli causes phasic dopamine release in the nucleus accumbens (NAc), a signaling event thought to be critical for initiation of motivated behaviors (Day et al., 2007; Grace, 1991; Oleson et al., 2012; Phillips et al., 2003a; Stuber et al., 2008).

The lateral habenula (LHb) is a key neuroanatomical regulator of midbrain reward circuitry. While dopaminergic neurons are excited by rewarding stimuli and inhibited by the omission of rewards, neurons in the LHb display contrary responses: they are inhibited by cues that predict rewards and excited by the omission of rewards (Matsumoto and Hikosaka, 2007). Importantly, in response to the omission of rewards, excitation of the LHb neurons precedes the inhibition of dopaminergic neurons, suggesting that LHb neurons may modulate VTA dopaminergic neurons. Further supporting this claim, electrical stimulation of the LHb inhibits midbrain dopaminergic neurons (Christoph et al., 1986; Ji and Shepard, 2007), while pharmacological inhibition of the LHb increases dopamine release in the striatum (Lecourtier et al., 2008). Collectively, these data suggest that LHb neurons encode negative reward prediction errors and may negatively modulate midbrain dopaminergic neurons in response to aversive events.

The LHb sends a functional glutamatergic projection to the rostromedial tegmental nucleus (RMTg, also referred to as the tail of the VTA), a population of GABAergic neurons located posterior to the VTA (Brinschwitz et al., 2010; Jhou et al., 2009; Stamatakis and Stuber, 2012). *In vivo* activation of VTA-projecting LHb neurons (Lammel et al., 2012), or LHb glutamatergic terminals in the RMTg, produces aversion and promotes motivated behavior to avoid further activation of the LHb-to-RMTg pathway (Stamatakis and Stuber, 2012), demonstrating a causal role for this pathway in controlling aversive behavior. Because GABAergic RMTg neurons inhibit midbrain dopaminergic neurons (Matsui and Williams, 2011), the RMTg is likely the intermediary structure through which the LHb inhibits midbrain dopaminergic neurons.

While the LHb-to-midbrain circuit has been dissected both functionally and behaviorally, less is known about the importance of the various LHb afferents. Inputs to the LHb arise from forebrain regions including the lateral hypothalamus, entopenduncular nucleus (EN), and prefrontal cortex (Kim and Lee, 2012; Poller et al., 2013; Shabel et al., 2012; Warden et al., 2012). A recent study suggests that aversive signaling by the LHb is mediated in part from the EN, as *in vivo* activation of these afferents in the LHb is aversive (Shabel et al., 2012). Although the majority of LHb afferents arise from the forebrain, the LHb also receives a substantial projection from the VTA (Gruber et al., 2007; Phillipson and Griffith, 1980; Skagerberg et al., 1984), with an estimated 30-50% of LHb-projecting VTA neurons being dopaminergic (Gruber et al., 2007; Skagerberg et al., 1984). Electrical stimulation of the midbrain decreases the firing rate of LHb neurons (Shen et al., 2012), but the functional and behavioral significance of synaptic inputs to the LHb arising from VTA dopaminergic neurons remains unknown. Here, we demonstrate that selective activation of this projection inhibits LHb neurons by the actions of synaptically released GABA, which disinhibits VTA dopaminergic neurons to promote reward-related behavior.

Results

Optogenetic targeting of VTA dopaminergic neurons and innervation to the LHb

To selectively target VTA dopaminergic neurons, we introduced a Cre-inducible viral construct coding for channelrhodopsin-2 fused to an enhanced yellow fluorescent protein (ChR2-eYFP) bilaterally into the VTA of *tyrosine hydroxylase* (*TH*)-internal ribosome entry site-Cre (*TH*^{VTA}: :ChR2) adult mice as previously described (Tsai et al., 2009). 3-4 weeks following surgery, we observed robust ChR2-eYFP expression in the VTA (Figure 1A,B). To ensure the specificity of ChR2-eYFP for dopaminergic neurons, we quantified the number of VTA neurons that were TH-positive (TH+) and eYFP-positive (eYFP+). We found that 62.4 ± 3.4% of VTA neurons were TH+, 48.6 ± 0.9% were eYFP+, and 99.2 ± 0.4% of the eYFP+ neurons were also labeled with TH (Figure 1C), consistent with previous results (Tsai et al., 2009). Six weeks following surgery, we observed eYFP expression that was largely restricted to the LHb relative to neighboring structures (Figure 1D,E). Fluorescence quantification analysis in brain slices containing the LHb revealed that axonal fibers originating from VTA dopaminergic neurons densely innervated the LHb, but only sparsely innervated surrounding structures, such as the medial habenula, thalamus, and hippocampus (Figure 1F).

LHb-projecting VTA dopaminergic neurons do not send axon collaterals to other reward-related brain structures

We next determined whether LHb-projecting VTA dopaminergic neurons (*TH*$^{VTA\text{-}LHb}$) collateralize and project to other brain regions. To accomplish this, we utilized an intersectional genetic approach to selectively label TH+ neurons in the VTA that project to the LHb. We bilaterally injected the LHb of *TH*-Cre mice with a retrogradely transducing herpes simplex virus (Chaudhury et al., 2013) encoding a Cre-inducible flippase recombinase (flp) under control the of an Ef1α promoter fragment (HSV-EF1α-LS1L-flp; Figure S1, see Supplemental Methods for more detail) (Kuhlman and Huang, 2008). In the same surgery, we bilaterally injected a flp-inducible ChR2-eYFP (AAV5-EF1α-fdhChR2(H134R)-eYFP; a novel construct designed with the same structure as the Cre-inducible viral construct coding for ChR2 (Tsai et al., 2009)) into the VTA (Figure 1G). This resulted in the selective labeling of the somas and processes of VTA TH+ neurons that project to the LHb. If *TH*$^{VTA\text{-}LHb}$ neurons collateralize to other target regions, we would expect to see eYFP+ fibers in these regions as well as the LHb. However, six weeks following this procedure, we observed eYFP+ fibers in the LHb, but not in other terminal regions of VTA dopaminergic neurons, such as the medial prefrontal cortex (mPFC), NAc, basolateral amygdala (BLA), or bed nucleus of the stria terminalis (BNST) (Figure 1G and Figure S1; n = 6 slices from n = 3 mice), suggesting that *TH*$^{VTA\text{-}LHb}$ neurons only project to the LHb, and do not send collaterals to these other target structures. Additionally, in a separate group of *TH*-Cre mice, we bilaterally injected the HSV-EF1α-LS1L-flp virus into the NAc and the AAV5-EF1α- fdhChR2(H134R)-eYFP virus into the VTA. In these mice, we observed eYFP+ fibers in the NAc, but not in the LHb (Figure S1, n = 6 slices from n = 3 mice).

TH$^{VTA\text{-}LHb}$ neurons are distinct from *TH*$^{VTA\text{-}NAc}$ neurons

To further confirm that *TH*$^{VTA\text{-}LHb}$ neurons are anatomically distinct from NAc-projecting VTA dopaminergic neurons (*TH*$^{VTA\text{-}NAc}$) and to provide an anatomical map of these discrete populations within the VTA, we performed retrograde tracing by injecting red fluorescent beads into the NAc and green fluorescent beads into the LHb of the same C57/BL6J wild-type mice (Figure 1H). Three weeks following surgery, VTA sections were collected and immunostained for TH. We found that *TH*$^{VTA\text{-}LHb}$ neurons were located in anterior and medial regions, congregating mainly in the interfasicular nucleus, while

TH$^{VTA-NAc}$ neurons were generally located more posterior and lateral (Figure 1I). Additionally, we observed significantly more *TH*$^{VTA-NAc}$ neurons than *TH*$^{VTA-LHb}$ neurons throughout the VTA (Figure 1I). Supporting our viral tracing data, we detected no TH+ neurons that expressed both red and green retrobeads in the VTA. Collectively, these data demonstrate that *TH*$^{VTA-LHb}$ and *TH*$^{VTA-NAc}$ neurons are completely separate neuronal populations.

Since we found that *TH*$^{VTA-NAc}$ and *TH*$^{VTA-LHb}$ neurons are separate populations of neurons within the VTA, we investigated whether these two populations display different electrophysiological characteristics. To accomplish this, we injected two groups of *TH*-GFP mice with red retrobeads either in the NAc or LHb and performed whole-cell recordings from GFP-positive neurons in VTA brain slices containing retrobeads (Figure 2A). Unlike *TH*$^{VTA-NAc}$ neurons, *TH*$^{VTA-LHb}$ neurons did not show a hyperpolarization-activated inward rectifying current (I_h), a traditional (though disputed) marker of midbrain dopaminergic neurons (Margolis et al., 2006; Mercuri et al., 1995) (Figure 2B). The lack of I_h, together with increased membrane resistance (Figure 2C), suggests that *TH*$^{VTA-LHb}$ neurons may be more excitable than *TH*$^{VTA-NAc}$ neurons. Supporting this observation, we found that *TH*$^{VTA-LHb}$ neurons show enhanced spontaneous activity compared to *TH*$^{VTA-NAc}$ neurons (Figure 2D,E).

A pharmacological signature of midbrain dopaminergic neurons is their hyperpolarization in response to D2 autoreceptor activation (Beckstead et al., 2004). To determine whether *TH*$^{VTA-LHb}$ neurons are sensitive to D2 autoreceptor activation, we performed cell-attached recordings from *TH*$^{VTA-LHb}$ and *TH*$^{VTA-NAc}$ neurons in the VTA. In line with previous data, we observed a significant decrease in spontaneous firing following a D2 receptor agonist (3 μM quinpirole) bath application in *TH*$^{VTA-NAc}$ neurons (Figure 2D-F; (Beckstead et al., 2004; Lammel et al., 2008)). However, quinpirole did not significantly change the spontaneous firing rate of *TH*$^{VTA-LHb}$ neurons (Figure 2D-F), demonstrating that *TH*$^{VTA-LHb}$ neurons lack functional somatodendritic D2 autoreceptors.

Since *TH*$^{VTA-LHb}$ and *TH*$^{VTA-NAc}$ neurons are anatomically and electrophysiologically distinct, we quantified the gene expression profiles of these two populations. To characterize the molecular phenotype of *TH*$^{VTA-LHb}$ and *TH*$^{VTA-NAc}$ neurons, we injected two groups of TH-GFP mice with red retrobeads either in the NAc or LHb and seven days later extracted the intracellular contents from individual GFP-positive neurons in VTA brain slices containing retrobeads (Figure 3A). The intracellular content was then processed by reverse transcription quantitative PCR assaying the following genes: *Vglut2* (vesicular glutamate transporter-2), *Vgat* (vesicular GABA transporter), *GAD1/GAD2* (glutamate decarboxylase 1 and 2), *Vmat2* (vesicular monoamine transporter-2), *DRD2,* (dopamine receptor D2), *DAT1* (dopamine transporter), and *TH* (tyrosine hydroxylase). We found that both *TH*$^{VTA-LHb}$ and *TH*$^{VTA-NAc}$ neurons expressed all tested genes classically associated with dopamine synthesis, release, and uptake (*Vmat2, DRD2, DAT1*, and *TH*; Figure 3B). However, *TH*$^{VTA-LHb}$ neurons expressed significantly lower amounts of *Vmat2, DRD2, and DAT1* compared to *TH*$^{VTA-NAc}$ neurons (Figure 3C). Importantly, none of these dopaminergic markers were detected in GFP negative neurons (n = 7 neurons). Taken together, these data suggest that *TH*$^{VTA-LHb}$ neurons are anatomically, electrophysiologically, and genetically distinct from *TH*$^{VTA-NAc}$ neurons.

Characterization of neurotransmitter release from *TH*$^{VTA-LHb}$ fibers

To characterize the dynamics of dopamine release from synaptic fibers that innervate the LHb, we performed fast-scan cyclic voltammetry in LHb brain slices obtained from *TH*^{VTA}: :ChR2 mice. Carbon-fiber microelectrodes were placed in areas within the LHb that displayed the highest ChR2-eYFP expression to ensure the voltammetry electrodes were

near presynaptic fibers and synapses that could be optically stimulated. We observed no detectable optically evoked dopamine release within the LHb, even after sustained high-frequency optical stimulation (Figure 4A-C). As positive controls, we recorded light-evoked dopamine release in NAc and BNST brain slices obtained from the same TH^{VTA}: :ChR2 mouse. We observed robust light-evoked dopamine release that increased as a function of either frequency or pulse number in both the NAc and BNST (Figure 4A-C), consistent with previous studies in the NAc and dorsal striatum of rats (Bass et al., 2013; Witten et al., 2011). We were unable to detect dopamine release in the LHb even after altering the parameters of the voltammetry experiments to increase the sensitivity of dopamine detection (Figure S2, see methods for additional details). Fluorescence quantification analysis of TH^{VTA}: :ChR2 fibers in the NAc, BNST, and LHb revealed that while the NAc had significantly higher eYFP fluorescence, there was no difference in eYFP intensity between the LHb and BNST (Figure 4D,E). These data suggest that the lack of detectable dopamine release in LHb brain slices is not likely due to weaker innervation, as we observed optically-evoked dopamine release in BNST slices which show comparable innervation.

In the NAc and BNST, we also observed intense TH immunofluorescence and a high degree of co-localization between eYFP+ fibers and TH immunostaining (Figure 4D,F) in brain slices obtained from TH^{VTA}: :ChR2 mice. In contrast, the LHb from the same mice exhibited strong eYFP fluorescence, but almost no TH immunoreactivity (Figure 4D,F). Quantitative analysis confirmed that co-localization (as assessed by Pearson's correlation coefficient) between eYFP and TH was 0.52 ± 0.05 for NAc and 0.50 ± 0.04 for the BNST, but only 0.010 ± 0.004 for the LHb. Together, these data suggest that fibers arising from VTA TH+ neurons express little or no TH in the fibers that innervate the LHb.

Because we did not observe dopamine release in the LHb, we sought to determine whether this projection might release other neurotransmitters in the LHb. In light of recent studies demonstrating that dopaminergic fibers can co-release glutamate and GABA in the striatum (Stuber et al., 2010; Tecuapetla et al., 2010; Tritsch et al., 2012), we asked whether fibers and synapses originating from TH^{VTA} neurons were capable of releasing either of these neurotransmitters in the LHb. Accordingly, we performed whole-cell voltage-clamped recordings from postsynaptic LHb neurons in brain slices obtained from TH^{VTA}: :ChR2 mice. To ensure we were only recording monosynaptic currents from TH^{VTA}: :ChR2 fibers, we added a Na^+-channel blocker (1 μM TTX) and a K^+-channel blocker (1 mM 4-AP) to the bath as previously described (Cruikshank et al., 2010). Voltage-clamp recordings from LHb neurons revealed that light pulses that selectively stimulated TH^{VTA}: :ChR2 fibers in the LHb ($TH^{VTA\text{-}LHb}$: :ChR2), produced light-evoked currents that were blocked by 10 μM of the $GABA_A$ receptor antagonist gabazine (Figure 5A-C). Of the neurons we recorded from in the LHb, 82% (45/55) received a direct monosynaptic inhibitory input from TH^{VTA} neurons. Dopaminergic terminals in the dorsal striatum release GABA that is dependent on *Vmat2* activity (Tritsch et al., 2012). However, we observed no changes in inhibitory currents in LHb slices from TH^{VTA}: :ChR2 mice treated with the *Vmat2* inhibitor reserpine, compared to untreated slices (Figure 5D). This same reserpine protocol was sufficient to inhibit electrically-evoked dopamine release in the NAc (Figure S3), demonstrating that this treatment was capable of inhibiting *Vmat2* and depleting evoked dopamine. These data demonstrate that $TH^{VTA\text{-}LHb}$ neurons do not require *Vmat2* function to release GABA in the LHb. Additionally, we observed a small (−7.2 ± 2.2 pA) excitatory current in some of the recorded neurons (5/10), consistent with a previous study demonstrating that *Vglut2*-expressing VTA neurons (some of which could be dopaminergic) innervate the LHb (Hnasko et al., 2012).

To determine whether activating $TH^{VTA\text{-}LHb}$: :ChR2 terminals would affect the spontaneous firing rate of postsynaptic LHb neurons, we performed cell-attached recordings from LHb

neurons and found that the average spontaneous firing rate of these neurons was 8.0 ± 2.2 Hz. When we delivered a 1-s 20-Hz optical pulse-train to optically stimulate $TH^{VTA\text{-}LHb}$: :ChR2 terminals, we observed that the firing rate of LHb neurons significantly decreased (Figure 5E-G), demonstrating that the net effect of $TH^{VTA\text{-}LHb}$: :ChR2 terminal stimulation was to suppress the firing of LHb neurons. To determine whether this suppression of firing was due to GABA or dopamine release, we added a D1/D2 receptor antagonist cocktail (10 μM SCH23390 and 10 μM raclopride) to the bath, followed by a $GABA_A$ receptor antagonist (10 μM gabazine). The D1/D2 receptor antagonist did not modify the decrease in firing in response to optical stimulation, but the $GABA_A$ receptor antagonist blocked this decrease, leading us to conclude that the inhibition of spontaneous firing following activation of $TH^{VTA\text{-}LHb}$: :ChR2 terminals is due to activation of $GABA_A$ receptors.

We performed electron microscopy to provide anatomical support for the electrophysiological findings. Accordingly, we collected images of $TH^{VTA\text{-}LHb}$: :ChR2 synapses (as defined by electron-dense DAB reaction product or silver-enhanced Nanogold after pre-embedding immunostaining for eYFP). Postembedding immunogold staining performed on this material showed that many of these presynaptic terminals contained high levels of GABA (Figure 5H). In some cases we also saw terminals containing little or no GABA that made asymmetric synaptic contacts (Figure S4; these were likely to be glutamatergic. Collectively, these congruous findings demonstrate that *TH*VTA-LHb: :ChR2 terminals do not release detectable amounts of dopamine in the LHb in an impulse-dependent fashion. Instead, $TH^{VTA\text{-}LHb}$: :ChR2 projections contain and release GABA, which functions to suppress the activity of postsynaptic LHb neurons.

The functional significance of the $TH^{VTA\text{-}LHb}$ circuit in regulating midbrain activity

Since the inhibitory $TH^{VTA\text{-}LHb}$ pathway suppresses the activity of postsynaptic LHb neurons (Figure 5E-G), we next addressed whether activation of this inhibitory circuit has downstream effects on midbrain activity *in vivo*. Given that the LHb sends a strong glutamatergic projection to the RMTg (Stamatakis and Stuber, 2012), we assessed the functional consequences of $TH^{VTA\text{-}LHb}$ activation on RMTg neuronal activity by recording extracellularly from RMTg neurons in anesthetized mice while stimulating $TH^{VTA\text{-}LHb}$ terminals (Figure 6A). Optical stimulation of the $TH^{VTA\text{-}LHb}$ pathway suppressed the spontaneous firing of RMTg neurons (Figure 6B-C). Further, these recorded RMTg units did not respond to optical stimulation within the RMTg (Figure S5), confirming that the recorded neurons did not express ChR2-eYFP. In agreement with this, we observed minimal ChR2-eYFP and TH+ immunolabeling in RMTg brain slices (Figure S5). Therefore, we considered these neurons to be *TH*-negative neurons, consistent with previous data (Barrot et al., 2012).

Because RMTg neurons directly inhibit VTA dopaminergic (TH^{VTA}) neurons (Matsui and Williams, 2011), we next determined if optical stimulation of $TH^{VTA\text{-}LHb}$ terminals would enhance TH^{VTA} neuronal activity via disinhibition. First, to optically classify recorded units as TH^{VTA} neurons, we recorded the firing responses of VTA neurons to the delivery of 2-ms light pulses within the VTA (Figure 6D-E). Optically- identified TH^{VTA} neurons displayed time-locked activation to VTA optical stimulation (Figure 6E-F).

Following identification of TH^{VTA} neurons, we determined whether optical stimulation of the $TH^{VTA\text{-}LHb}$ inhibitory pathway (by delivering 473 nm light directly into the LHb) could alter the spontaneous activity of TH^{VTA} neurons. Optical stimulation of $TH^{VTA\text{-}LHb}$ terminals led to enhanced spontaneous activity in optically identified TH^{VTA} neurons (Figure 6G-H). Importantly, we determined that these light-evoked responses were unlikely to arise from antidromic activation of $TH^{VTA\text{-}LHb}$ terminals, as $TH^{VTA\text{-}LHb}$ initiated spikes

had significantly longer spike latencies and greater spike jitter compared to the light-evoked spikes of TH^{VTA} neurons with direct optical stimulation in the VTA (Figure 6I). Furthermore, TH^{VTA} neurons did not respond reliably to 20-Hz optical stimulation of $TH^{VTA\text{-}LHb}$ terminals (Figure 6J). Collectively, these data suggest that the increases in firing of TH^{VTA} neurons initiated by $TH^{VTA\text{-}LHb}$ terminal activation are mediated through synaptic transmission within a polysynaptic circuit. Taken together, these circuit-activity mapping experiments reveal the functional significance of the inhibitory $TH^{VTA\text{-}LHb}$ pathway in regulating midbrain activity.

Optogenetic activation of the $TH^{VTA\text{-}LHb}$ pathway produces reward-related behavioral phenotypes that require $GABA_A$ signaling

In vivo, pharmacological inhibition of the LHb increases dopamine in forebrain regions such as the striatum (Lecourtier et al., 2008). Likewise, we observed that *in vivo* activation of the $TH^{VTA\text{-}LHb}$ pathway increased the firing rate of midbrain dopaminergic neurons (Figure 6). Therefore, we hypothesized that *in vivo* activation of the $TH^{VTA\text{-}LHb}$: :ChR2 pathway would result in a reward-related phenotype. To test this hypothesis, we implanted bilateral optical fibers (Sparta et al., 2012) aimed directly above the LHb in $TH^{VTA\text{-}LHb}$: :ChR2 mice (Figure S6) and determined the behavioral ramifications of selectively activating the $TH^{VTA\text{-}LHb}$: :ChR2 pathway. Using a real-time place preference assay, as previously described (Stamatakis and Stuber, 2012), $TH^{VTA\text{-}LHb}$: :ChR2 mice exhibited a significant preference for the side of the chamber that was paired with optical stimulation. In contrast, litter-mate controls ($TH^{VTA\text{-}LHb}$: :Control), displayed no preference, demonstrating that activation of the $TH^{VTA\text{-}LHb}$: :ChR2 pathway produces reward-related behaviors (Figure 7A-C). This preference was dependent on $GABA_A$ signaling within the LHb, as intra-LHb microinjections of a $GABA_A$ receptor antagonist (gabazine) through guide cannulas interfaced with the optical fibers (Jennings et al., 2013) blocked the preference for the stimulation-paired side (Figure 7D, Figure S7). In contrast, intra-LHb microinjection of a dopamine receptor antagonist (D1 and D2) cocktail did not block the rewarding phenotype (Figure 7D, Figure S7), while a systemic injection of the dopamine antagonist cocktail did disrupt the preference (Figure 7E, Figure S7). These data suggest that the observed reward-related phenotype induced by optical stimulation of $TH^{VTA\text{-}LHb}$: :ChR2 pathway does not depend on dopamine signaling within the LHb, but rather on downstream dopamine signaling in brain regions such as the NAc. Finally, to determine if activation of the $TH^{VTA\text{-}LHb}$: :ChR2 pathway is reinforcing, we trained mice to nose-poke for optical stimulation of the $TH^{VTA\text{-}LHb}$: :ChR2 pathway (Figure 7F-H). $TH^{VTA\text{-}LHb}$: :ChR2 mice made significantly more nose-pokes to receive optical stimulation than $TH^{VTA\text{-}LHb}$: :control mice (Figure 7F-H).

Taken together, these data demonstrate that while activation of $TH^{VTA\text{-}LHb}$: :ChR2 terminals does not result in detectable dopamine release in the LHb, selective activation of this pathway promotes reward-related behavior by suppressing LHb activity through the release of GABA, leading to disinhibition of VTA dopaminergic neurons.

Discussion

Aberrant mesolimbic and mesocortical dopaminergic signaling has been implicated in a range of neuropsychiatric diseases, including schizophrenia, addiction, and depression (Chaudhury et al., 2013; Knable and Weinberger, 1997; Lüscher and Malenka, 2011; Phillips et al., 2003b; Tye et al., 2013), motivating extensive studies of VTA dopaminergic projections to the striatum and prefrontal cortex. In contrast, little is known about the VTA's projection to the LHb. Using optogenetics in combination with electrophysiology,

genetically targeted neuronal tracing techniques, and behavior, we investigated the functional and behavioral significance of this mesohabenular pathway.

Previous studies have demonstrated that separate populations of VTA dopaminergic neurons project to non-overlapping target structures such as the NAc, BLA, and mPFC (Ford et al., 2006; Lammel et al., 2008; Swanson, 1982). Our data are consistent with these findings, demonstrating that $TH^{VTA\text{-}LHb}$ neurons do not collateralize to the NAc, BLA, PFC, or BNST. We also found that $TH^{VTA\text{-}LHb}$ neurons display electrophysiological characteristics distinct from $TH^{VTA\text{-}NAc}$ neurons. Notably, we found that $TH^{VTA\text{-}LHb}$ neurons are more excitable than $TH^{VTA\text{-}NAc}$ neurons, are insensitive to D2 autoreceptor activation, and do not display an I_h current, an electrophysiological characteristic often used to identify a neuron as dopaminergic in slice electrophysiological experiments (Mercuri et al., 1995). Recent studies have demonstrated that although NAc-projecting and BLA-projecting VTA dopaminergic neurons typically have robust I_h currents, dopaminergic neurons that project to the mPFC lack I_h currents and functional somatodendritic D2 autoreceptors (Ford et al., 2006; Lammel et al., 2008, 2011). Collectively, these data support the idea that VTA dopaminergic neurons are not a homogenous population, as they can vary greatly depending on their electrophysiological markers and their projection targets.

Although $TH^{VTA\text{-}LHb}$ neurons express TH mRNA and show TH immunostaining in the soma (Figure 1H, Figure 3), we observed only very weak TH expression in $TH^{VTA\text{-}LHb}$: :ChR2 fibers and terminals (Figure 4D). Consistent with this, voltammetric methods failed to detect released dopamine in the LHb following optical stimulation of $TH^{VTA\text{-}LHb}$: :ChR2 fibers. It is worth noting that we observed dense core vesicles in presynaptic terminals originating from $TH^{VTA\text{-}LHb}$ neurons (Figure 5H). Previous work has demonstrated that the vesicular monoamine transporter can be associated with dense core vesicles in VTA neurons, suggesting that dopamine may be contained in both clear synaptic vesicles and dense core vesicles (Nirenberg et al., 1996). It is possible that a low content of dopamine within the dense core vesicles in the LHb could be released following specific stimulation patterns, leading to concentrations of dopamine in the LHb too low to detect with voltammetric methods. Additionally, since TH is being produced in the soma, $TH^{VTA\text{-}LHb}$ neurons may be releasing dopamine locally from the somatodendritic compartment, which could then activate D2 autoreceptors to modulate the firing rate of neighboring VTA neurons (Adell and Artigas, 2004).

Previous studies have found that systemic injections of dopaminergic agonists, and bath-application of high concentrations of dopamine, result in changes in the firing patterns and glucose utilization of LHb neurons (Jhou et al., 2013; Kowski et al., 2009; McCulloch et al., 1980). However, as dopaminergic agonists often have affinities for serotonin receptors (Newman-Tancredi et al., 2002), which are thought to reside on presynaptic terminals in the LHb (Shabel et al., 2012), it is unclear whether the effects of these agonists on LHb activity arise from direct activation of dopamine receptors in the LHb.

LHb neurons exhibit a high basal firing rate both in slices (Figure 5; Jhou et al., 2013) and *in vivo* (Bromberg-Martin et al., 2010; Meier and Herrling, 1993), which likely exerts a tonic inhibitory influence on dopaminergic neurons by activating RMTg GABAergic neurons that directly inhibit VTA dopaminergic neurons. Supporting this hypothesis, we found that inhibition of LHb neurons through activation of $TH^{VTA\text{-}LHb}$: :ChR2 terminals decreased RMTg firing and increased the spontaneous firing rate of VTA dopaminergic neurons (Figure 6), consistent with previous data demonstrating that pharmacological inhibition of the LHb increases dopamine release in the forebrain (Lecourtier et al., 2008). LHb neurons show a decrease in firing in response to cues that predict rewards (Matsumoto and Hikosaka, 2007). Thus, we suggest that the phasic dopamine release seen in the NAc in response to

motivationally relevant stimuli, at least in part, could require activation of inhibitory afferents to LHb, thus disinhibiting midbrain dopaminergic neurons. Data presented here demonstrate that a hybrid population of VTA neurons expressing dopaminergic and GABAergic markers send an inhibitory projection to the LHb, and thus are able to directly inhibit LHb neurons, resulting in profound downstream effects on midbrain circuitry. This provides a circuit mechanism by which activation of the VTA-to-LHb pathway could promote reward.

Along with a robust excitatory projection to GABAergic neurons in the RMTg and posterior VTA, the LHb also sends a modest direct glutamatergic projection to VTA dopaminergic neurons (Balcita-Pedicino et al., 2011; Stamatakis and Stuber, 2012). If the VTA dopaminergic neurons that receive a direct connection from the LHb also project back to the LHb, this could provide an elegant negative feedback mechanism, whereby activation of the LHb would result in activation of $TH^{\text{VTA-LHb}}$ neurons, which in turn would shut down LHb activity.

While the presence of a mesohabenular pathway has been recognized for many years (Phillipson and Griffith, 1980; Swanson, 1982), the present study is the first to characterize the behavioral and functional relevance of this pathway. Our data adds to the mounting evidence that dopaminergic neurons within the VTA are heterogeneous with respect to their electrophysiological and molecular profiles, their projection targets, and neurotransmitter signaling modalities. Further, our data demonstrate that the LHb and midbrain interact in a reciprocal manner and implicate the VTA's projection to the LHb as a key node in the classical midbrain reward circuit. This mechanistic framework underscores the flexibility and complexity of the circuitry that impinges upon VTA dopaminergic neurons to promote motivated behavior.

Experimental Procedures

Subjects and stereotactic surgery

Adult (25-30 g) mice were group housed until surgery and maintained on a reverse 12-hr light cycle (lights off at 8:00) with *ad libitum* access to food and water. Mice were anesthetized with ketamine (150 mg/kg of body weight) and xylazine (50 mg/kg) and placed in a stereotactic frame (Kopf Instruments). For all slice electrophysiology and fast-scan cyclic voltammetry experiments, except for the retrobeads experiments, male and female *TH*-IRES-Cre backcrossed to C57BL/6J were bilaterally microinjected with 0.5 μL of purified and concentrated adeno-associated virus serotype 5 (AAV5; ~10^{12} infections units per mL, packaged and titered by the UNC Vector Core Facility) into the VTA. Stereotactic coordinates are available in the Supplemental Experimental Procedures. Each VTA was injected with an AAV5 coding Cre-inducible ChR2 under control of the EF1 α promoter to transduce VTA dopaminergic neurons ($TH^{\text{VTA-}}$: :ChR2). For the retrobead slice electrophysiology and PCR retrobead experiments, male and female *TH*-IRES-GFP mice received quadruple injections of 0.3 μL of red retrobeads (Lumafluor) into either the NAc or LHb. For the retrobead mapping and quantification experiments, male C57BL/6J mice (Jackson Laboratory, Bar Harbor ME) received quadruple injections with 0.3 μL of red retrobeads into the NAc. In the same surgery, the mice also received quadruple injections of 0.3 μL with green retrobeads (Lumafluor) into the LHb. For tracing experiments, *TH*-IRES-Cre mice were bilaterally injected with 0.5 μL of HSV-EF1α-LS1L-flp into the LHb or NAc and bilaterally injected with 0.5 μL of AAV5-EF1α-fdhChR2(H134R)-eYFP into the VTA. A detailed description of the HSV vector construction is available in the Supplemental Experimental Procedures. For behavioral experiments, male *TH*-IRES-Cre positive ($TH^{\text{VTA-LHb}}$: :ChR2) and negative ($TH^{\text{VTA-LHb}}$: :Control) littermates were bilaterally injected with Cre-inducible ChR2 and also implanted with bilateral chronic fibers directed

above the LHb. For the LHb microinjection experiments, a 26-gauge steel tube cannula (McMasters-Carr) that terminated 0.5 mm above the tip of the optical fiber was epoxied to an optical fiber and bilaterally aimed at the LHb. Retrobead experiments were performed 7-21 days after surgery. All other experiments were performed 6-8 weeks after surgery. Histology, immunohistochemistry, confocal, and electron microscopy procedures can be found in the Supplemental Experimental Procedures. All procedures were conducted in accordance with the Guide for the Care and Use of Laboratory Animals, as adopted by the US National Institutes of Health, and with approval of the UNC Institutional Animal Care and Use Committees.

Slice preparation for single-cell reverse transcription PCR, fast-scan cyclic voltammetry, and patch-clamp electrophysiology

Mice were anesthetized with pentobarbital and perfused transcardially with modified artificial cerebrospinal fluid. Electrophysiological solutions can be found in the Supplemental Experimental Procedures. Brains were then rapidly removed and placed in the same solution that was used for perfusion at ~0° C. For the PCR experiments, horizontal slices containing the VTA (200 μm) were cut on a Vibratome (VT-1200, Leica Microsystems). For fast-scan cyclic voltammetry, coronal slices containing either the NAc (250 μm), (BNST 250 um), or LHb (250 μm) were obtained. For patch-clamp electrophysiology, coronal slices containing the LHb (200 μm), or horizontal slices containing the VTA (200 μm) were obtained. Following slicing, brain slices were placed in a holding chamber and were allowed to recover for at least 30 min before being placed in the recording chamber and superfused with bicarbonate-buffered solution saturated with 95% O_2 and 5% CO_2.

Reverse transcription PCR

Electrophysiological solutions, equipment, and recording procedures can be found in the Supplemental Experimental Procedures. Autoclaved patch electrodes (2.0-2.5 MΩ) were backfilled with approximately 3-5 μL of a potassium chloride internal solution. 2 μL of RNAse inhibitor (ANTI-RNase, Life Technologies) was added per 1 mL of the potassium chloride internal solution. Holding current was measured for no more than 3 minutes to minimize potential mRNA degradation. The cytoplasm was then aspirated by applying negative pressure and the integrity of the seal was monitored during aspiration to prevent extracellular contamination. Cells that showed more than a 100-pA change in holding current during aspiration were discarded. Immediately following aspiration, the pipette was removed from the tissue and the tip was broken into an RNAse-free PCR tube. The solution inside the pipette was then injected into the RNAse-free tube using positive pressure. Between each cell recording, the silver wire located inside the recording pipette was wiped thoroughly with 70% alcohol to minimize cross sample contamination. Finally, to control for pipette contamination, after each 5 consecutive recordings, a recording pipette was lowered into the tissue with positive pressure, but without aspiration (tissue-stick control) and was then processed for qPCR. Single-cell gene expression profiling and single-cell gene analysis are described in the Supplemental Experimental Procedures.

Fast-scan cyclic voltammetry

Equipment, recording procedures, and analysis can be found in the Supplemental Experimental Procedures. T-650 carbon fiber microelectrodes (100-200 μm in length) were used for detection of dopamine in brain slices. Electrodes were placed in the NAc core, dorsal lateral BNST, or LHb of TH^{VTA}: :ChR2 brain slices. Every 100 ms, the potential applied to the electrode was ramped from −0.4 V to +1.3 V to −0.4 V versus a Ag/AgCl reference wire at a rate of 400 V/s. To increase the sensitivity to detect dopamine with fast-

scan cyclic voltammetry, slices were prepared as described above, but were incubated in aCSF containing 1 μM GBR12909 and 10 μM raclopride for at least 1 h before recording. Prior to recording, slices were pre-perfused with L-Dopa (10 μM) for 10 min. Additionally, the electrode was ramped from −0.6 to 1.4 V to −0.6 V versus a Ag/AgCl reference wire at a rate of 400 V/s.

Patch-clamp electrophysiology

Electrophysiological solutions, equipment, recording procedures, and bath-applications of drugs can be found in the Supplemental Experimental Procedures. For the retrobeads experiments, whole-cell voltage clamp and cell-attached recordings were made from GFP+ neurons containing red retrobeads in the VTA. I_h current was measured by voltage-clamping the cell and stepping from -70mV to −105 mV in 5 mV steps. For voltage-clamp recordings in LHb neurons, membrane potentials were maintained at −70 mV, and light pulses were delivered every 20 s to evoke neuronal firing. For cell-attached recordings, a 20-Hz optical stimulation was delivered for 1 s every 20 s for 20 sweeps. Firing rate was averaged across all 20 sweeps.

In vivo circuit activity mapping of the $TH^{VTA\text{-}LHb}$ pathway

Surgical procedures, recordings, and analysis are described in the Supplemental Experimental Procedures. For monitoring RMTg and VTA neural firing during optical stimulation of the $TH^{VTA\text{-}LHb}$ pathway, the recording electrode was lowered separately into the RMTg (−3.9 mm posterior to bregma, +/−0.9 mm lateral to midline, and −3.6 mm ventral to skull surface) and VTA (−3.1 mm posterior to bregma, +/−0.4 mm lateral to midline, and −5.0 mm ventral to skull surface) by a motorized micromanipulator (Scientifica). To optically stimulate $TH^{VTA\text{-}LHb}$ terminals, an optical fiber coupled to a solid state laser (473 nm) was situated within a guide cannula and placed directly above the LHb at a 15° angle (−1.7 mm posterior to bregma, +/−1.25 mm lateral to midline, and −3.24 mm ventral to skull surface). 20-Hz train pulses of light were delivered to the LHb every 3 s for 20 trials (each trial having 2-s pre-stimulation, 2-s stimulation, and 1-s post-stimulation periods; Off, On, Off). To optically stimulate RMTg and VTA cell bodies, an optical fiber was fed through the side port of the electrode holder to terminate near the tip of the glass recording electrode. Recorded units were classified as light-responsive neurons if reliable light-evoked spikes were detected during the presentation of 2-ms light pulses (20 trials each).

In vivo optogenetic experiments

Real-time place preference procedures, optical self-stimulation and 5-choice self-stimulation procedures were conducted as previously described (Jennings et al., 2013; Stamatakis and Stuber, 2012, see Supplemental Experimental Procedures).

Supplementary Material

Refer to Web version on PubMed Central for supplementary material.

Acknowledgments

We thank V. Gukassyan and the UNC Neuroscience Center Microscopy Core (P30 NS045892), and the members of the Stuber laboratory for discussion. We thank Kristen Phend and Susan Burette for technical assistance with histology and electron microscopy. We thank the UNC Vector Core Facility for viral packaging. This study was supported by The Whitehall Foundation, NARSAD, The Foundation of Hope, and National Institutes of Health grants DA032750 (to G.D.S), DA034472 (to A.M.S), and NS039444 (to R.J.W.)

References

Adell A, Artigas F. The somatodendritic release of dopamine in the ventral tegmental area and its regulation by afferent transmitter systems. Neuroscience & Biobehavioral Reviews. 2004; 28:415–431. [PubMed: 15289006]

Balcita-Pedicino JJ, Omelchenko N, Bell R, Sesack SR. The inhibitory influence of the lateral habenula on midbrain dopamine cells: ultrastructural evidence for indirect mediation via the rostromedial mesopontine tegmental nucleus. J Comp Neurol. 2011; 519:1143–1164. [PubMed: 21344406]

Barrot M, Sesack SR, Georges F, Pistis M, Hong S, Jhou TC. Braking Dopamine Systems: A New GABA Master Structure for Mesolimbic and Nigrostriatal Functions. J Neurosci. 2012; 32:14094–14101. [PubMed: 23055478]

Bass CE, Grinevich VP, Kulikova AD, Bonin KD, Budygin EA. Terminal effects of optogenetic stimulation on dopamine dynamics in rat striatum. J Neurosci Methods. 2013; 214:149–155. [PubMed: 23391758]

Beckstead MJ, Grandy DK, Wickman K, Williams JT. Vesicular Dopamine Release Elicits an Inhibitory Postsynaptic Current in Midbrain Dopamine Neurons. Neuron. 2004; 42:939–946. [PubMed: 15207238]

Brinschwitz K, Dittgen A, Madai VI, Lommel R, Geisler S, Veh RW. Glutamatergic axons from the lateral habenula mainly terminate on GABAergic neurons of the ventral midbrain. Neuroscience. 2010; 168:463–476. [PubMed: 20353812]

Bromberg-Martin ES, Matsumoto M, Hikosaka O. Distinct tonic and phasic anticipatory activity in lateral habenula and dopamine neurons. Neuron. 2010; 67:144–155. [PubMed: 20624598]

Chaudhury D, Walsh JJ, Friedman AK, Juarez B, Ku SM, Koo JW, Ferguson D, Tsai HC, Pomeranz L, Christoffel DJ, et al. Rapid regulation of depression-related behaviours by control of midbrain dopamine neurons. Nature. 2013; 493:532–536. [PubMed: 23235832]

Christoph GR, Leonzio RJ, Wilcox KS. Stimulation of the lateral habenula inhibits dopamine-containing neurons in the substantia nigra and ventral tegmental area of the rat. J Neurosci. 1986; 6:613–619. [PubMed: 3958786]

Cohen JY, Haesler S, Vong L, Lowell BB, Uchida N. Neuron-type-specific signals for reward and punishment in the ventral tegmental area. Nature. 2012; 482:85–88. [PubMed: 22258508]

Cruikshank SJ, Urabe H, Nurmikko AV, Connors BW. Pathway-specific feedforward circuits between thalamus and neocortex revealed by selective optical stimulation of axons. Neuron. 2010; 65:230–245. [PubMed: 20152129]

Day JJ, Roitman MF, Wightman RM, Carelli RM. Associative learning mediates dynamic shifts in dopamine signaling in the nucleus accumbens. Nat Neurosci. 2007; 10:1020–1028. [PubMed: 17603481]

Ford CP, Mark GP, Williams JT. Properties and Opioid Inhibition of Mesolimbic Dopamine Neurons Vary according to Target Location. J Neurosci. 2006; 26:2788–2797. [PubMed: 16525058]

Grace AA. Phasic versus tonic dopamine release and the modulation of dopamine system responsivity: a hypothesis for the etiology of schizophrenia. Neuroscience. 1991; 41:1–24. [PubMed: 1676137]

Gruber C, Kahl A, Lebenheim L, Kowski A, Dittgen A, Veh RW. Dopaminergic projections from the VTA substantially contribute to the mesohabenular pathway in the rat. Neurosci Lett. 2007; 427:165–170. [PubMed: 17949902]

Hnasko TS, Hjelmstad GO, Fields HL, Edwards RH. Ventral tegmental area glutamate neurons: electrophysiological properties and projections. J Neurosci. 2012; 32:15076–15085. [PubMed: 23100428]

Jennings JH, Sparta DR, Stamatakis AM, Ung RL, Pleil KE, Kash TL, Stuber GD. Distinct extended amygdala circuits for divergent motivational states. Nature. 2013

Jhou TC, Geisler S, Marinelli M, Degarmo BA, Zahm DS. The mesopontine rostromedial tegmental nucleus: A structure targeted by the lateral habenula that projects to the ventral tegmental area of Tsai and substantia nigra compacta. J Comp Neurol. 2009; 513:566–596. [PubMed: 19235216]

Jhou TC, Good CH, Rowley CS, Xu SP, Wang H, Burnham NW, Hoffman AF, Lupica CR, Ikemoto S. Cocaine drives aversive conditioning via delayed activation of dopamine-responsive habenular and midbrain pathways. J Neurosci. 2013; 33:7501–7512. [PubMed: 23616555]

Ji H, Shepard PD. Lateral habenula stimulation inhibits rat midbrain dopamine neurons through a GABA(A) receptor-mediated mechanism. J Neurosci. 2007; 27:6923–6930. [PubMed: 17596440]

Kim U, Lee T. Topography of descending projections from anterior insular and medial prefrontal regions to the lateral habenula of the epithalamus in the rat. European Journal of Neuroscience. 2012; 35:1253–1269. [PubMed: 22512256]

Knable MB, Weinberger DR. Dopamine, the prefrontal cortex and schizophrenia. J Psychopharmacol (Oxford). 1997; 11:123–131. [PubMed: 9208376]

Kowski AB, Veh RW, Weiss T. Dopaminergic activation excites rat lateral habenular neurons in vivo. Neuroscience. 2009; 161:1154–1165. [PubMed: 19374940]

Kuhlman SJ, Huang ZJ. High-resolution labeling and functional manipulation of specific neuron types in mouse brain by Cre-activated viral gene expression. PLoS ONE. 2008; 3:e2005. [PubMed: 18414675]

Lammel S, Hetzel A, Häckel O, Jones I, Liss B, Roeper J. Unique Properties of Mesoprefrontal Neurons within a Dual Mesocorticolimbic Dopamine System. Neuron. 2008; 57:760–773. [PubMed: 18341995]

Lammel S, Ion DI, Roeper J, Malenka RC. Projection-specific modulation of dopamine neuron synapses by aversive and rewarding stimuli. Neuron. 2011; 70:855–862. [PubMed: 21658580]

Lammel S, Lim BK, Ran C, Huang KW, Betley MJ, Tye KM, Deisseroth K, Malenka RC. Input-specific control of reward and aversion in the ventral tegmental area. Nature. 2012; 491:212–217. [PubMed: 23064228]

Lecourtier L, Defrancesco A, Moghaddam B. Differential tonic influence of lateral habenula on prefrontal cortex and nucleus accumbens dopamine release. Eur J Neurosci. 2008; 27:1755–1762. [PubMed: 18380670]

Lüscher C, Malenka RC. Drug-evoked synaptic plasticity in addiction: from molecular changes to circuit remodeling. Neuron. 2011; 69:650–663. [PubMed: 21338877]

Margolis EB, Lock H, Hjelmstad GO, Fields HL. The ventral tegmental area revisited: is there an electrophysiological marker for dopaminergic neurons? J Physiol (Lond). 2006; 577:907–924. [PubMed: 16959856]

Margolis EB, Coker AR, Driscoll JR, Lemaître AI, Fields HL. Reliability in the identification of midbrain dopamine neurons. PLoS ONE. 2010; 5:e15222. [PubMed: 21151605]

Matsui A, Williams JT. Opioid-sensitive GABA inputs from rostromedial tegmental nucleus synapse onto midbrain dopamine neurons. J Neurosci. 2011; 31:17729–17735. [PubMed: 22131433]

Matsumoto M, Hikosaka O. Lateral habenula as a source of negative reward signals in dopamine neurons. Nature. 2007; 447:1111–1115. [PubMed: 17522629]

McCulloch J, Savaki HE, Sokoloff L. Influence of dopaminergic systems on the lateral habenular nucleus of the rat. Brain Research. 1980; 194:117–124. [PubMed: 7378832]

Meier C, Herrling P. N-Methyl-D-Asparate induces regular firing patterns in the cat lateral habenula in vivo. Neuroscience. 1993; 52:951–959. [PubMed: 7680802]

Mercuri NB, Bonci A, Calabresi P, Stefani A, Bernardi G. Properties of the Hyperpolarization-activated Cation Current lh in Rat Midbrain Dopaminergic Neurons. European Journal of Neuroscience. 1995; 7:462–469. [PubMed: 7773443]

Newman-Tancredi A, Cussac D, Quentric Y, Touzard M, Verrièle L, Carpentier N, Millan MJ. Differential Actions of Antiparkinson Agents at Multiple Classes of Monoaminergic Receptor III Agonist and Antagonist Properties at Serotonin, 5-HT1 and 5-HT2, Receptor Subtypes. J Pharmacol Exp Ther. 2002; 303:815–822. [PubMed: 12388668]

Nirenberg MJ, Chan J, Liu Y, Edwards RH, Pickel VM. Ultrastructural Localization of the Vesicular Monoamine Transporter-2 in Midbrain Dopaminergic Neurons: Potential Sites for Somatodendritic Storage and Release of Dopamine. J Neurosci. 1996; 16:4135–4145. [PubMed: 8753875]

Oleson EB, Gentry RN, Chioma VC, Cheer JF. Subsecond dopamine release in the nucleus accumbens predicts conditioned punishment and its successful avoidance. J Neurosci. 2012; 32:14804–14808. [PubMed: 23077064]

Pan WX, Schmidt R, Wickens JR, Hyland BI. Dopamine cells respond to predicted events during classical conditioning: evidence for eligibility traces in the reward-learning network. J Neurosci. 2005; 25:6235–6242. [PubMed: 15987953]

Phillips PEM, Stuber GD, Heien MLAV, Wightman RM, Carelli RM. Subsecond dopamine release promotes cocaine seeking. Nature. 2003a; 422:614–618. [PubMed: 12687000]

Phillips PEM, Stuber GD, Heien MLAV, Wightman RM, Carelli RM. Subsecond dopamine release promotes cocaine seeking. Nature. 2003b; 422:614–618. [PubMed: 12687000]

Phillipson OT, Griffith AC. The neurones of origin for the mesohabenular dopamine pathway. Brain Res. 1980; 197:213–218. [PubMed: 7397554]

Poller WC, Madai VI, Bernard R, Laube G, Veh RW. A glutamatergic projection from the lateral hypothalamus targets VTA-projecting neurons in the lateral habenula of the rat. Brain Res. 2013

Schultz W, Dayan P, Montague PR. A Neural Substrate of Prediction and Reward. Science. 1997; 275:1593–1599. [PubMed: 9054347]

Shabel SJ, Proulx CD, Trias A, Murphy RT, Malinow R. Input to the lateral habenula from the basal ganglia is excitatory, aversive, and suppressed by serotonin. Neuron. 2012; 74:475–481. [PubMed: 22578499]

Shen X, Ruan X, Zhao H. Stimulation of midbrain dopaminergic structures modifies firing rates of rat lateral habenula neurons. PLoS ONE. 2012; 7:e34323. [PubMed: 22485164]

Skagerberg G, Lindvall O, Björklund A. Origin, course and termination of the mesohabenular dopamine pathway in the rat. Brain Res. 1984; 307:99–108. [PubMed: 6087992]

Sparta DR, Stamatakis AM, Phillips JL, Hovelsø N, Van Zessen R, Stuber GD. Construction of implantable optical fibers for long-term optogenetic manipulation of neural circuits. Nat Protoc. 2012; 7:12–23. [PubMed: 22157972]

Stamatakis AM, Stuber GD. Activation of lateral habenula inputs to the ventral midbrain promotes behavioral avoidance. Nat Neurosci. 2012; 15:1105–1107. [PubMed: 22729176]

Stuber GD, Klanker M, De Ridder B, Bowers MS, Joosten RN, Feenstra MG, Bonci A. Reward-predictive cues enhance excitatory synaptic strength onto midbrain dopamine neurons. Science. 2008; 321:1690–1692. [PubMed: 18802002]

Stuber GD, Hnasko TS, Britt JP, Edwards RH, Bonci A. Dopaminergic terminals in the nucleus accumbens but not the dorsal striatum corelease glutamate. J Neurosci. 2010; 30:8229–8233. [PubMed: 20554874]

Swanson LW. The projections of the ventral tegmental area and adjacent regions: a combined fluorescent retrograde tracer and immunofluorescence study in the rat. Brain Res Bull. 1982; 9:321–353. [PubMed: 6816390]

Tecuapetla F, Patel JC, Xenias H, English D, Tadros I, Shah F, Berlin J, Deisseroth K, Rice ME, Tepper JM, et al. Glutamatergic signaling by mesolimbic dopamine neurons in the nucleus accumbens. J Neurosci. 2010; 30:7105–7110. [PubMed: 20484653]

Tobler PN, Fiorillo CD, Schultz W. Adaptive Coding of Reward Value by Dopamine Neurons. Science. 2005; 307:1642–1645. [PubMed: 15761155]

Tritsch NX, Ding JB, Sabatini BL. Dopaminergic neurons inhibit striatal output through non-canonical release of GABA. Nature. 2012; 490:262–266. [PubMed: 23034651]

Tsai HC, Zhang F, Adamantidis A, Stuber GD, Bonci A, De Lecea L, Deisseroth K. Phasic firing in dopaminergic neurons is sufficient for behavioral conditioning. Science. 2009; 324:1080–1084. [PubMed: 19389999]

Tye KM, Mirzabekov JJ, Warden MR, Ferenczi EA, Tsai HC, Finkelstein J, Kim SY, Adhikari A, Thompson KR, Andalman AS, et al. Dopamine neurons modulate neural encoding and expression of depression-related behaviour. Nature. 2013; 493:537–541. [PubMed: 23235822]

Ungless MA, Magill PJ, Bolam JP. Uniform inhibition of dopamine neurons in the ventral tegmental area by aversive stimuli. Science. 2004; 303:2040–2042. [PubMed: 15044807]

Warden MR, Selimbeyoglu A, Mirzabekov JJ, Lo M, Thompson KR, Kim SY, Adhikari A, Tye KM, Frank LM, Deisseroth K. A prefrontal cortex-brainstem neuronal projection that controls response to behavioural challenge. Nature. 2012; 492:428–432. [PubMed: 23160494]

Witten IB, Steinberg EE, Lee SY, Davidson TJ, Zalocusky KA, Brodsky M, Yizhar O, Cho SL, Gong S, Ramakrishnan C, et al. Recombinase-driver rat lines: tools, techniques, and optogenetic application to dopamine-mediated reinforcement. Neuron. 2011; 72:721–733. [PubMed: 22153370]

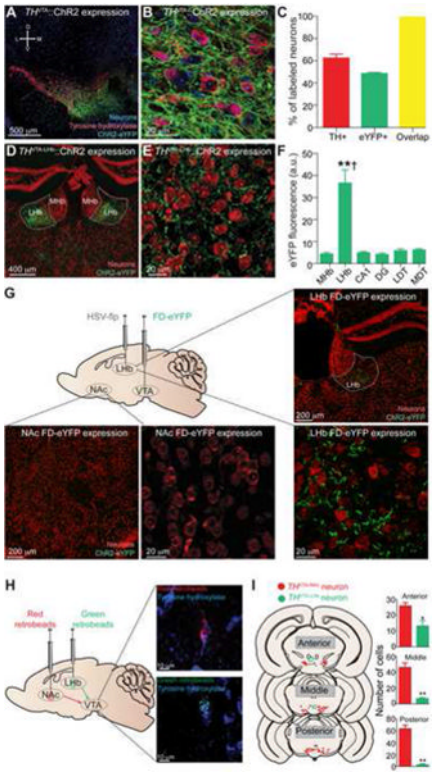

Figure 1. *TH*$^{\text{VTA-LHb}}$ neurons are a distinct population of neurons

(A,B) Confocal images of coronal sections showing expression of ChR2-eYFP in the VTA following injection of Cre-inducible virus into the VTA of a *TH*-IRES-Cre (*TH*$^{\text{VTA}}$: :ChR2) mouse. (C) Quantification of TH+, eYFP+, and eYFP+ neurons that are also TH+ (n = 4 sections from n = 3 mice). (D,E) Confocal images of coronal sections showing expression of ChR2-eYFP fibers in the LHb of a *TH*$^{\text{VTA}}$: :ChR2 mouse. (F) eYFP fluorescence intensity is significantly higher in the LHb than in surrounding regions ($F[5,30] = 5.718$, $p < 0.0001$; n = 6 sections from n = 3 mice). MHb = medial habenula; LHb = lateral habenula; DG = dentate gyrus; LDT = lateral dorsal thalamus; MDT = medial dorsal thalamus. (G) Diagram illustrates HSV-EF1α-LS1L-flp (HSV-flp) and AAV5-EF1α-fdhChR2(H134R)-eYFP (FD-eYFP) viral injections. Confocal images show eYFP expression in the NAc (below) and LHb (right) following injection of HSV-flp into the LHb and FD-eYFP into the VTA of *TH*:IRES:Cre mice. See also Figure S1. (H) Left: schematic of retrobead injections. Right: confocal images of separate TH+ neurons containing NAc-injected beads (top) and LHb-injected beads (bottom). (I) Left: Location of *TH*$^{\text{VTA-NAc}}$ neurons (red) and *TH*$^{\text{VTA-LHb}}$ neurons (green) from a representative animal. Right: More TH+ neurons in the VTA contained red retrobeads (*TH*$^{\text{VTA-NAc}}$ neurons) than green retrobeads *(TH*$^{\text{VTA-LHb}}$ neurons) (Anterior: $t[8] = 3.01$, $p = 0.02$; n = 5 sections from n = 4 mice. Middle: $t[8] = 6.51$, $p = 0.0002$; n = 5 sections from n = 4 mice. Posterior: $t[6] = 9.58$, $p < 0.0001$; n = 4 sections from n = 4 mice). Error bars represent s.e.m. **$p < 0.01$ (Student's t-test and ANOVA followed by Bonferroni post-hoc comparisons, where applicable). Dagger symbol denotes significance compared to all manipulations.

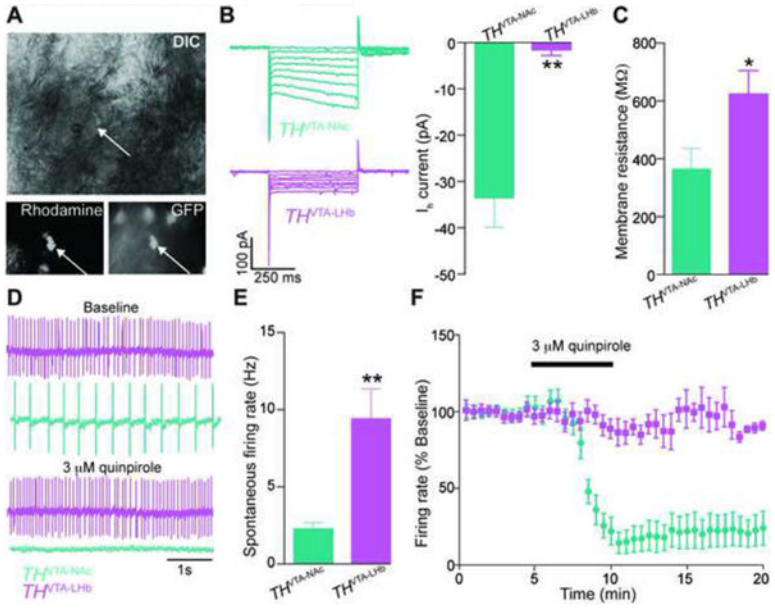

Figure 2. *TH*$^{\text{VTA-LHb}}$ neurons exhibit distinct electrophysiological characteristics

(A) Top: VTA neuron (indicated by arrow) visualized with a DIC microscope. Bottom left: same neuron visualized under epifluorescent illumination with rhodamine filter. Bottom right: same neuron visualized under epifluorescent illumination with GFP filter. (B) Left: representative traces showing I_h current in a *TH*$^{\text{VTA-NAc}}$ neuron (top) and *TH*$^{\text{VTA-LHb}}$ neuron (bottom) in response to voltage steps. Right: *TH*$^{\text{VTA-LHb}}$ neurons show significantly less I_h current than *TH*$^{\text{VTA-NAc}}$ neurons (t[16] = 4.5, p = 0.0004; n=10 *TH*$^{\text{VTA-NAc}}$ neurons and 8 *TH*$^{\text{VTA-LHb}}$ neurons). (C) *TH*$^{\text{VTA-LHb}}$ neurons have a higher membrane resistance than *TH*$^{\text{VTA-NAc}}$ neurons (t[16] = 2.4, p = 0.03; n=10 *TH*$^{\text{VTA-NAc}}$ neurons and 8 *TH*VTA-LHb neurons) (D) Representative traces showing spontaneous firing of *TH*$^{\text{VTA-NAc}}$ neuron (purple) and *TH*$^{\text{VTA-LHb}}$ neuron (green) during a baseline period (top) and following a bath application of a D2 agonist (3 μM quinpirole, bottom). (E) Spontaneous firing is significantly higher in *TH*$^{\text{VTA-LHb}}$ neurons than in *TH*$^{\text{VTA-NAc}}$ neurons (t[17] = 3.78, p = 0.0015; n=10 *TH*$^{\text{VTA-NAc}}$ neurons and 9 *TH*$^{\text{VTA-LHb}}$ neurons. (F) 3 μM bath application of quinpirole decreases the spontaneous firing rate significantly more for *TH*$^{\text{VTA-NAc}}$ neurons compared to *TH*$^{\text{VTA-LHb}}$ neurons (F[34,490] = 10.58, p = < 0.0001; n = 9 *TH*$^{\text{VTA-NAc}}$ neurons and 7 *TH*$^{\text{VTA-LHb}}$ neurons. Error bars represent s.e.m. *p < 0.05 **p < 0.01 (Student's t-test and ANOVA followed by Bonferroni post-hoc comparisons, where applicable).

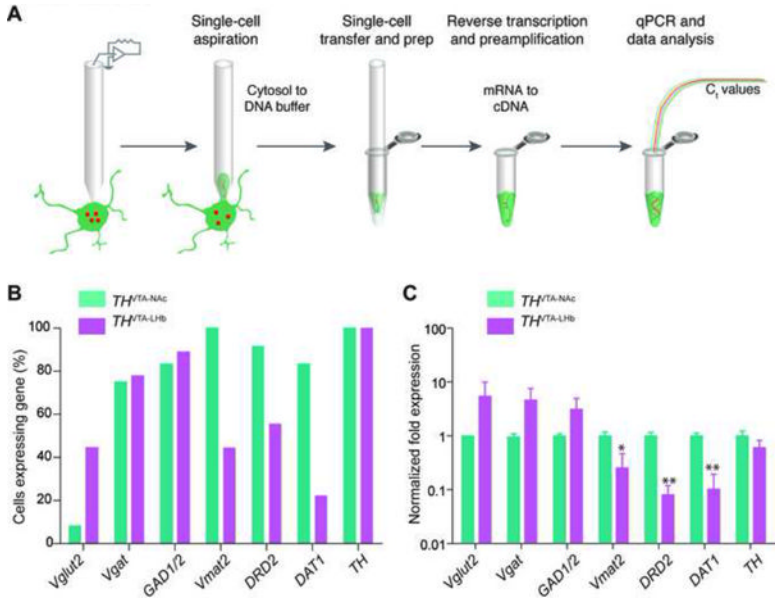

Figure 3. *TH*$^{VTA-LHb}$ neurons express lower amounts of mRNA for dopaminergic markers than *TH*$^{VTA-NAc}$ neurons

(A) Schematic of single-cell reverse transcription quantitative PCR analysis. (B) Percentage of *TH*$^{VTA-LHb}$ and *TH*$^{VTA-NAc}$ neurons expressing each gene (*Vglut2*, vesicular glutamate transporter-2; *Vgat*, vesicular GABA transporter; *GAD1/GAD2*, glutamate decarboxylase 1 and 2; *Vmat2*, vesicular monoamine transporter-2; *DRD2*, dopamine receptor D2; *DAT1*, dopamine transporter; and *TH*, tyrosine hydroxylase). (C) C_t values for each target gene were normalized to the control gene expressed in all neurons, *Rn18s*, and log transformed fold expression values represent single cell expression relative to *TH*$^{VTA-NAc}$ expression. The average fold expression for *Vmat2*, *DRD2*, and *DAT1* is significantly lower in *TH*$^{VTA-LHb}$ neurons compared *TH*$^{VTA-NAc}$ neurons (*Vmat2*: U = 19, p = 0.0136; *DRD2*: U = 10, p = 0.0053; *DAT1*: U = 17.00, p = 0.0069; n = 9 *TH*$^{VTA-LHb}$ neurons from n = 4 mice and n = 12 *TH*$^{VTA-NAc}$ neurons from n = 3 mice. Error bars represent s.e.m. *p < 0.05 **p < 0.01 (Mann-Whitney).

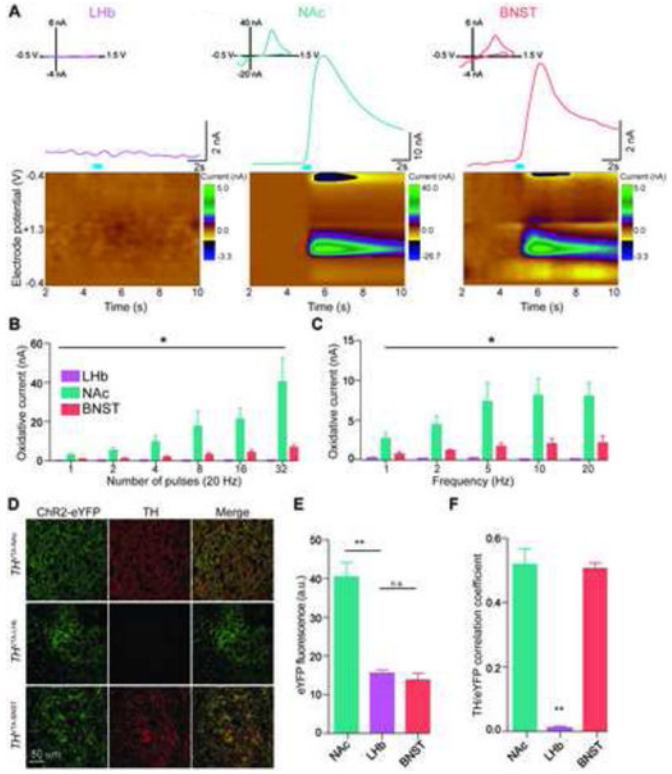

Figure 4. $TH^{VTA\text{-}LHb}$ neurons do not release detectable levels of dopamine in the LHb

(A) Fast-scan cyclic voltammetric recordings of optically-evoked dopamine release in LHb (left), NAc (middle), and BNST (right) brain slices from TH^{VTA}: :ChR2 mice. Top: Example traces of voltammetric recordings from LHb (left), NAc (middle), and BNST (right) brain slices. Insets: Background-subtracted cyclic voltammograms showing an electrochemical signal indicative of oxidized dopamine in the NAc and BNST, but not in the LHb. Bottom: Consecutive background-subtracted voltammograms recorded over the 8-s interval. Applied potential (E_{apps} versus Ag/AgCl reference electrode) is shown on Y-axis. Time at which each voltammogram was recorded is shown on X-axis. Current changes are color-coded. (B) Light-evoked current is significantly higher in the NAc than LHb at 20Hz for all measured number of pulses ($F[5,1] = 19.1$, $p < 0.0001$). Light-evoked current is significantly higher in the BSNT than LHb at 20 Hz for 8,16, and 32 pulses ($F[5,1] = 72.59$, $p < 0.0001$). (C) Light-evoked current is significantly higher in the NAc than LHb for all measured frequencies ($F[4,1] = 29.11$, $p < 0.001$). Light-evoked current is significantly higher in the BNST than LHb for 10 and 20 Hz ($F[4,1] = 25.43$, $p < 0.001$). See also Figure S2. (D) Confocal images showing eYFP- and TH-expression in the NAc (top), LHb (middle), and BNST (bottom) from TH^{VTA}: :ChR2 coronal sections. (E) eYFP fluorescence intensity is significantly higher in the NAc than in the LHb ($t[10] = 6.58$, $p < 0.0001$). eYFP fluorescence intensity is not significantly different between the LHb and BNST ($t[10] = 0.9002$, $p = 0.389$). n = 6 slices/region from n = 3 mice (F) ChR2-eYFP and TH co-localize significantly less in the LHb than in the BNST and NAc (Pearson's Correlation Coefficient, $F[2,12] = 76.49$, $p < 0.0001$; n = 5 slices/region from n = 3 mice). Error bars represent s.e.m. **$p < 0.01$ (Student's t-test and ANOVA followed by Bonferroni post-hoc comparisons, where applicable).

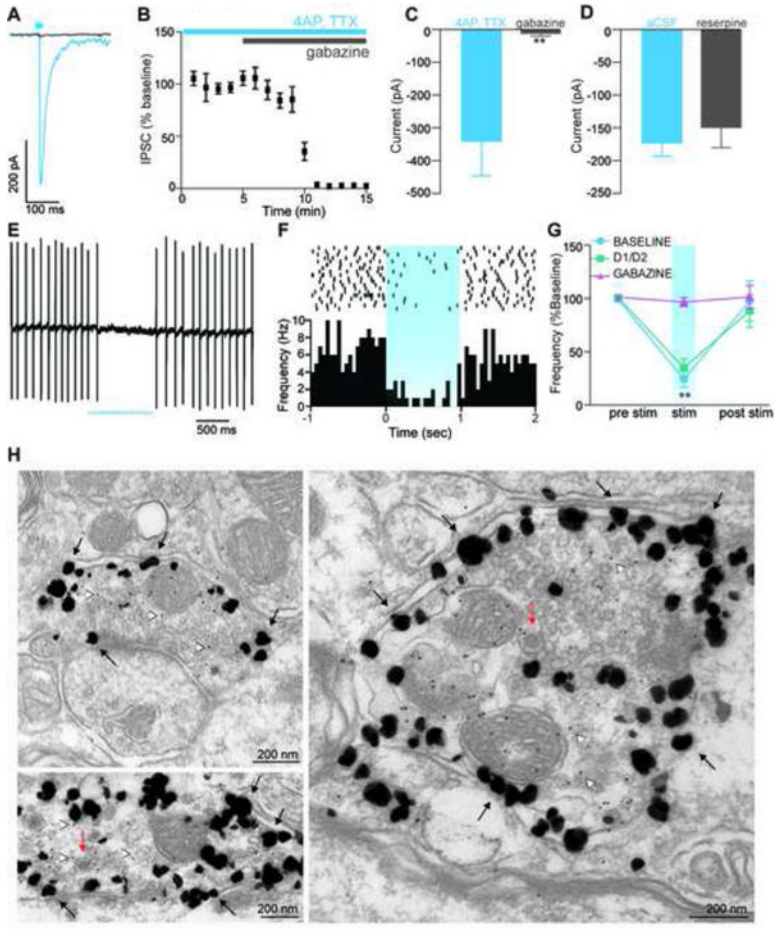

Figure 5. *TH*$^{\text{VTA-LHb}}$ neurons release GABA in the LHb

(A-C) Light-evoked IPSCs recorded from LHb neurons in the presence of 1 mM 4-AP and 1 μM TTX are blocked by bath-application of 10 μM gabazine ($t(12) = 3.12$, $p = 0.009$; $n = 7$ neurons). (D) Light-evoked IPSCs recorded from LHb neurons in normal aCSF and from reserpine-treated mice ($t[18] = 0.60$; $p = 0.56$; $n = 10$ neurons each). See also Figure S3 (E-G) Cell-attached recording demonstrating a significant decrease in spontaneous firing rate of LHb neurons in response to a 1-s 20-Hz optical stimulation of *TH*$^{\text{VTA-LHb}}$: :ChR2 terminals in the LHb in normal aCSF (Baseline: $t[14] = 9.57$, $p < 0.0001$) and after application of a D1/D2 antagonist (D1/D2: $t[14] = 7.76$, $p < 0.0001$), but not after application of a $GABA_A$ receptor antagonist (gabazine: $t[14] = 1.05$, $p = 0.31$) $n = 10$ neurons. (H) Electron micrographs showing *TH*$^{\text{VTA-LHb}}$: :ChR2 fibers, as defined by large silver-enhanced nanogold particles (black arrows) containing GABA (detected with 10 nm gold particles, white arrows). *TH*$^{\text{VTA-LHb}}$: :ChR2 fibers also contain dense-core vesicles (red arrows). See also Figure S4. Error bars represent s.e.m. **$p < 0.01$ (Student's t-test and ANOVA followed by Bonferroni post-hoc comparisons, where applicable).

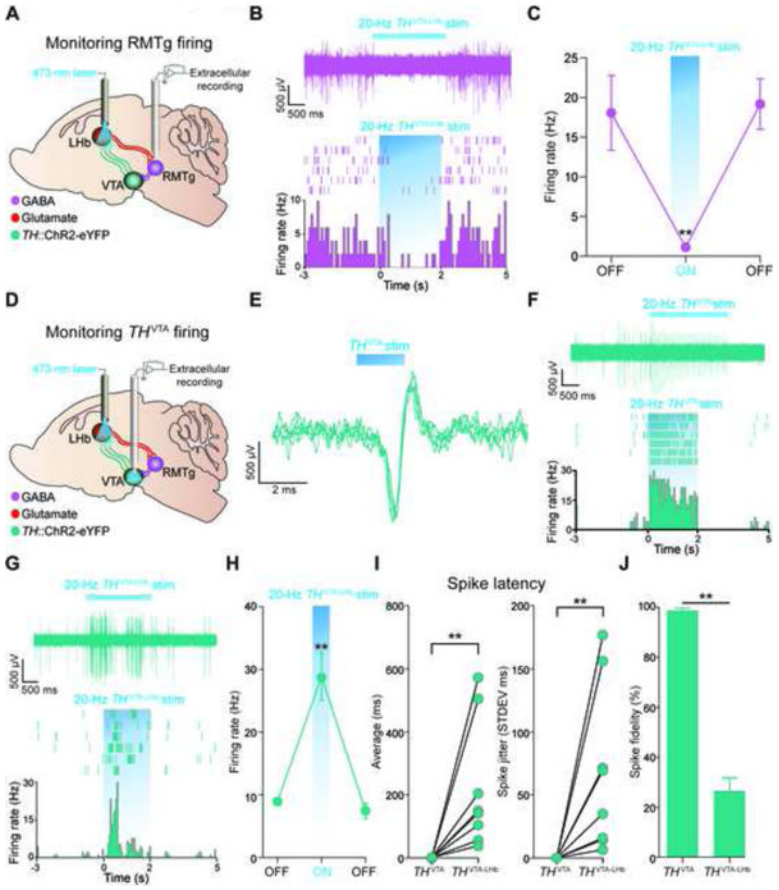

Figure 6. *In vivo* optical stimulation of $TH^{VTA\text{-}LHb}$ terminals suppresses RMTg activity and enhances spontaneous firing of TH^{VTA} neurons

(A) A schematic depicting anesthetized *in vivo* electrophysiological recordings from RMTg neurons during $TH^{VTA\text{-}LHb}$ terminal optical stimulation. (B) Example trace from a single RMTg unit (top) and its representative peri-event histogram and raster (bottom) demonstrating repeated attenuation of firing to 20-Hz optical stimulation of the $TH^{VTA\text{-}LHb}$ pathway. (C) Off, On, Off: before, during, after 20-Hz photostimulation (3 s each; 20 trials). The average firing rate of RMTg units significantly decreased during the 3-s 20-Hz optical stimulation trials ($F[2,15] = 4.33$, $p = 0.03$, n = 3 mice, n = 6 units). See also Figure S5. (D) Schematic for anesthetized *in vivo* extracellular recordings in the VTA. (E) Example traces from a single optically-tagged TH^{VTA} unit displaying repeated time-locked activation to 2-ms optical stimulation of the VTA. (F) Example trace from a single TH^{VTA} unit (top) and its representative peri-event histogram and raster (bottom) displaying repeated time-locked activation to 20-Hz optical stimulation of TH^{VTA} cell bodies. (G) Example trace from a single TH^{VTA} unit (top) and its representative peri-event histogram and raster (bottom) displaying enhanced activity in response to 20-Hz optical stimulation of $TH^{VTA\text{-}LHb}$ terminals within the LHb. (H) The average firing rate of optically-identified TH^{VTA} units significantly increased during the 20-Hz optical stimulation trials ($F[2,12] = 10.02$, $p = 0.0028$, n = 3 mice, n = 5 units). (I) The average latency of each optical stimulation parameter (soma vs. terminal; left) demonstrates that optical stimulation of $TH^{VTA\text{-}LHb}$ terminals resulted in significantly greater spike latencies in optically-identified TH^{VTA} neurons compared to light-evoked spikes from TH^{VTA}-soma optical stimulation ($p = 0.0053$, n = 3 mice, n = 9 units). The standard deviation (STDEV) of each stimulation type (right) shows that light-evoked spikes from TH^{VTA}-soma optical stimulation displayed significantly

greater latency stability compared to $TH^{VTA\text{-}LHb}$-initiated spikes ($p = 0.0014$, $n = 3$ mice, $n = 9$ units). (J) TH^{VTA}-soma light-evoked spikes responded more reliably to 20-Hz optical stimulation compared to $TH^{VTA\text{-}LHb}$-terminal light-evoked spikes ($F[1,18] = 11.2$, $p = 0.0036$, $n = 3$ mice, $n = 11$ units). Error bars represent s.e.m. $^{**}p < 0.01$ (Student's t-test and ANOVA followed by Bonferroni post-hoc comparisons, where applicable).

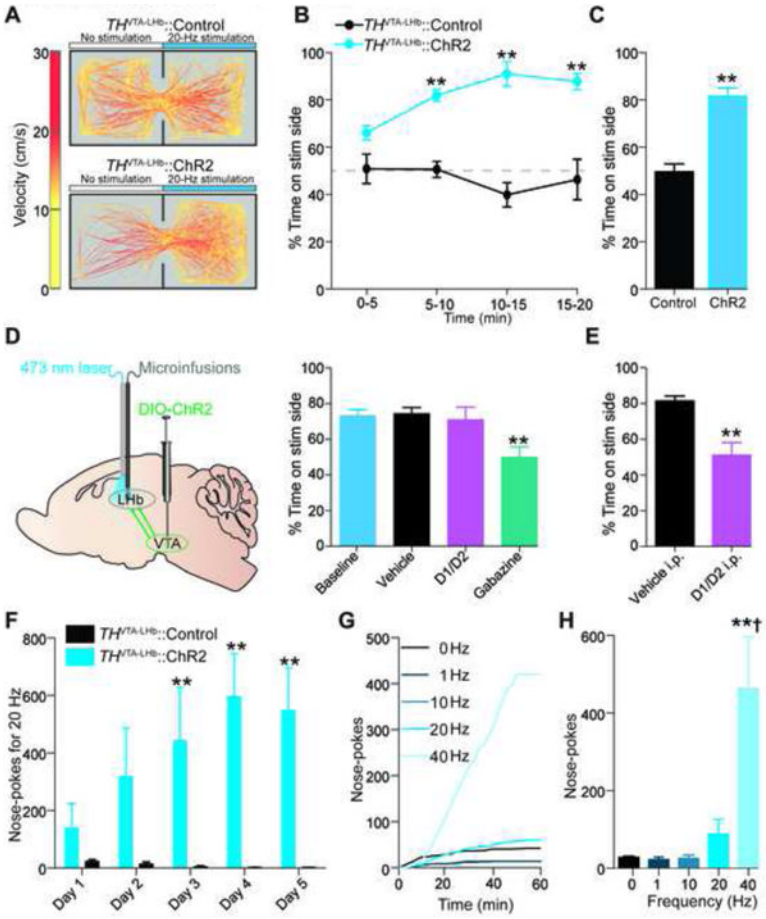

Figure 7. Activation of *TH*$^{VTA-LHb}$ terminals produces reward-related behavioral phenotypes

(A) Representative tracks from *TH*$^{VTA-LHb}$: :Control (top) and *TH*$^{VTA-LHb}$: :ChR2 (bottom) mice during RTPP task. (B,C) *TH*$^{VTA-LHb}$: :ChR2 mice spent more time on the side of the chamber paired with stimulation than *TH*$^{VTA-LHb}$: :Control mice (5 minute time bins: $F[3,1] = 79.2$, $p < 0.0001$; entire 20-min session: $t[13] = 8.82$, $p<0.0001$; n=8 *TH*$^{VTA-LHb}$: :Control and 7 *TH*$^{VTA-LHb}$: :ChR2). See also Figure S6. (D) Intra-LHb injections of a $GABA_A$ antagonist, but not a dopamine receptor (D1 and D2) antagonist cocktail, followed by *TH*$^{VTA-LHb}$: :ChR2 stimulation blocked the real-time place preference ($F[3,32] = 5.1$, $p = 0.005$; n = 9 mice). (E) Systemic injection of a dopamine receptor (D1 and D2) antagonist cocktail followed by *TH*$^{VTA-LHb}$: :ChR2 stimulation blocked the real-time place preference ($t[12] = 4.0$, $p = 0.002$; n = 7 mice). (F) Active nose-poke responses from *TH*$^{VTA-LHb}$: :ChR2 and *TH*$^{VTA-LHb}$: :Control mice over the first 4 days of training. *TH*$^{VTA-LHb}$: :ChR2 mice made significantly more nose-pokes on Day 3, 4, and 5 than *TH*$^{VTA-LHb}$: :Control mice (Day 3: $t[12] = 3.78$, $p < 0.01$; Day 4: $t[12] = 4.45$, $p < 0.001$; Day 5: $t[12] = 4.22$, $p <0.001$). (G) Example cumulative records of nose-pokes made by a TH$^{VTA-LHb}$: :ChR2 mouse for 0-, 1-, 10-, 20- and 40-Hz optical stimulation in the 5-choice nose-poke task. (H) *TH*$^{VTA-LHb}$: :ChR2 mice made significantly more nose-pokes for 40 Hz than any other frequency ($F[4,25] = 9.13$, $p < 0.0001$). n = 6 *TH*$^{VTA-LHb}$: :ChR2 mice. n = 8 *TH*$^{VTA-LHb}$: :Control mice. Dagger symbol denotes significance compared to all manipulations. Error bars represent s.e.m. **p < 0.01 (Student's t-test and ANOVA followed by Bonferroni post-hoc comparisons, where applicable). See also Figure S7.